

Article

Molecular Self-Assembly of an Unusual Dinuclear Ruthenium(III) Complex Based on the Nucleobase Guanine

Marta Orts-Arroyo, Adriana Silvestre-Llora, Isabel Castro  and José Martínez-Lillo * 

Instituto de Ciencia Molecular (ICMol), Universitat de València, c/Catedrático José Beltrán 2, Paterna, 46980 València, Spain; marta.orts-arroyo@uv.es (M.O.-A.); asillo@alumni.uv.es (A.S.-L.); isabel.castro@uv.es (I.C.)
* Correspondence: f.jose.martinez@uv.es; Tel.: +34-9635-44460

Abstract: The study of crystal structures based on complexes containing purine nucleobases is a significant research subject, mainly regarding the diagnosis and treatment of some diseases and the investigation of genetic mutations and biochemical structures in life sciences. We have obtained and characterized a new dinuclear ruthenium(III) complex based on guanine with the formula $[\{\text{Ru}(\mu\text{-Cl})(\mu\text{-gua})\}_2\text{Cl}_4]\cdot 2\text{H}_2\text{O}$ (**1**) (gua = guanine). **1** was characterized by means of Fourier transform infrared spectroscopy (FT-IR), scanning electron microscopy and energy dispersive X-ray analysis (SEM-EDX), single-crystal X-ray diffraction (XRD), Hirshfeld surface analysis and cyclic voltammetry (CV). The study of its electrochemical properties allowed us to investigate the presence of guanine molecules when linked to the ruthenium(III) ion in **1**. The well-resolved voltammetric response together with the reliability and stability achieved through **1** could provide a step forward to developing new ruthenium-based platforms, devices and modified electrodes adequate to study this purine nucleobase.

Keywords: guanine; ruthenium; FT-IR spectroscopy; Hirshfeld surface; SEM-EDX; cyclic voltammetry



Citation: Orts-Arroyo, M.; Silvestre-Llora, A.; Castro, I.; Martínez-Lillo, J. Molecular Self-Assembly of an Unusual Dinuclear Ruthenium(III) Complex Based on the Nucleobase Guanine. *Crystals* **2022**, *12*, 448. <https://doi.org/10.3390/cryst12040448>

Academic Editors: Ana M. Garcia-Deibe and Jesús Sanmartín-Matalobos

Received: 7 March 2022

Accepted: 18 March 2022

Published: 23 March 2022

Publisher's Note: MDPI stays neutral with regard to jurisdictional claims in published maps and institutional affiliations.

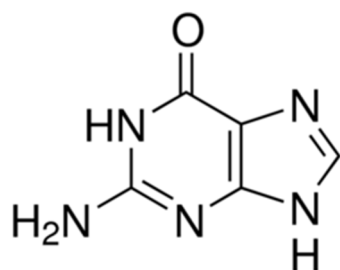


Copyright: © 2022 by the authors. Licensee MDPI, Basel, Switzerland. This article is an open access article distributed under the terms and conditions of the Creative Commons Attribution (CC BY) license (<https://creativecommons.org/licenses/by/4.0/>).

1. Introduction

Guanine is one of the main nitrogenous bases found in the nucleotides of the nucleic acids (DNA and RNA) present in the cells of living organisms and viruses. Besides being involved in the storage and the expression of genetic information, it participates in many other cellular biochemical processes and structures [1–3]. Given that this purine nucleobase can be present in the fluids of human beings, their levels have been proposed as direct and indirect biomarkers for a variety of diseases and pathologies, such as Alzheimer's disease [4], epilepsy [5] and human immunodeficiency virus (HIV) infection [6,7]. Hence, sensitive and selective methods for determining both this and other purine nucleobases are being investigated in several research areas [8,9].

Ruthenium complexes have undergone significant development in different research areas for the last 20 years [10], displaying a wide variety of technological applications, and ranging from catalysis to anticancer drugs [11–18]. Following our ongoing investigation into biomolecule-based complexes [19–27], we have focused also on the purine nucleobase guanine (Scheme 1). There exists only one guanine-containing Ru(III) complex, of the formula *trans*- $[\text{RuCl}_4(\text{Hgua})(\text{DMSO})]\cdot 2\text{H}_2\text{O}$ (Hgua = protonated guanine), which was reported in 2004 [28]. This compound was characterized by single-crystal X-ray diffraction and its *in vitro* antitumor activity was also evaluated, showing a mild antiproliferative effect but an interesting proadhesive effect [28]. Herein, we report the synthesis and characterization of a new guanine-bridged diruthenium(III) complex, of formula $[\{\text{Ru}(\mu\text{-Cl})(\mu\text{-gua})\}_2\text{Cl}_4]\cdot 2\text{H}_2\text{O}$ (**1**) (gua = guanine). To our knowledge, **1** is the first dinuclear ruthenium(III) compound based on guanine which has been reported so far.



Scheme 1. Molecular structure of guanine.

2. Materials and Methods

2.1. Reagents and Instruments

Guanine (99.90%) was purchased from Acros Organics and the ruthenium precursor $K_2[RuCl_5(H_2O)]$ (99.95%) was acquired from Alfa Aesar. The elemental analyses (C, H, N) and X-ray microanalysis were performed through Central Service for the Support to Experimental Research (SCSIE) at the University of Valencia. Images and results of scanning electron microscopy (SEM-EDX) were obtained through a Hitachi S-4800 field emission scanning electron microscope, with 20 kV and 9.0 mm of accelerating voltage and working distance, respectively. Each infrared spectrum (FT-IR) was performed on KBr pellets and was obtained through a PerkinElmer Spectrum 65 FT-IR spectrometer in the 4000–500 cm^{-1} range with 25 scans and a spectral resolution of 4 cm^{-1} . The study of the electrochemical properties was carried out on **1** by means of an Autolab/PGSTAT 204 scanning potentiostat at a scan rate working in the 10–250 range (mVs^{-1}) and with Metrohm electrodes. CV curves were obtained with a 0.1 M $(NBu_4)[PF_6]$ solution, as supporting electrolyte, and a 10^{-3} M solution of **1** in dry *N,N'*-dimethylformamide (DMF). A glassy carbon disk of 0.32 cm^2 was used as working electrode, polished with 1.0 μm diamond powder, which was sonicated and then washed with absolute ethanol and acetone, and air-dried. The AgCl/Ag reference electrode was separated from the test solution through a salt bridge with the solvent and supporting electrolyte. The platinum electrode was auxiliary. The study was performed in a standard electrochemical cell at 20 °C with flowing argon. The studied potential range was from -1.5 to $+1.5$ V vs. AgCl/Ag. Ferrocene (Fc) was added as an internal standard at the end of the measurements.

2.2. Preparation

Synthesis of $[Ru(\mu-Cl)(\mu-gua)_2Cl_4] \cdot 2H_2O$ (**1**)

$K_2[RuCl_5(H_2O)]$ (11.2 mg, 0.03 mmol) and guanine (6.80 mg, 0.03 mmol) were reacted through a solvothermal synthesis in HCl (4 mL, 3.0 M) at 90 °C for three days, then a 12 h cooling process took place to room temperature. Dark brown parallelepipeds of **1** were obtained. Yield: ca. 53%. Anal. Calcd. for $C_{10}H_{10}Cl_6N_{10}O_2Ru_2$ (**1**): C, 16.8; H, 1.4; N, 19.5. Found: C, 16.7; H, 1.7; N, 19.2. SEM-EDX: a molar ratio of 1:3 for Ru/Cl was found for **1**. IR peaks (KBr pellets): 3419(s), 3325(m), 3208(m), 3114(m), 3062(m), 3012(m), 2922(m), 2853(m), 1708(vs), 1635(vs), 1594(m), 1559(m), 1540(s), 1506(w), 1457(m), 1394(s), 1270(w), 1210(m), 1124(w), 1095(w), 983(w), 873(m), 768(m), 704(w), 612(w), 573(w), 474(w) cm^{-1} .

2.3. X-ray Diffraction Data Collection and Structure Refinement

Data collection from a single crystal of **1** (with dimensions of $0.46 \times 0.13 \times 0.09$ mm^3) was performed on a Bruker D8 Venture diffractometer with graphite-monochromated $Mo-K_{\alpha}$ radiation ($\lambda = 0.71073$ Å). Table 1 summarizes the crystal parameters and refinement results for **1**. The structure of **1** was solved by standard direct methods and then completed by Fourier recycling through the SHELXTL program. The model was refined with version 2018/1 of SHELXL against F^2 on all data by full-matrix least-squares [29]. The non-hydrogen atoms were anisotropically refined, and the H atoms of the guanine molecules were set in calculated positions and refined isotropically. The H atoms of the water molecules in **1** were neither detected nor included in the model, this fact being due

to the thermal disorder observed on the water molecules, which increases the R_1 and wR_2 parameters in this system (Table 1). The graphic manipulations were performed with the DIAMOND program [30] of CCDC 2081706.

Table 1. Summary of the crystal data and structure refinement parameters for **1** (see Supplementary Material).

Compound	1
CIF	2081706
Formula	$C_{10}H_{10}Cl_6N_{10}O_4Ru_2$
$M_r/g\ mol^{-1}$	749.12
Crystal system	Monoclinic
Space group	$C2/c$
$a/\text{\AA}$	22.462(4)
$b/\text{\AA}$	11.330(2)
$c/\text{\AA}$	12.446(2)
$\alpha/^\circ$	90
$\beta/^\circ$	122.42(1)
$\gamma/^\circ$	90
$V/\text{\AA}^3$	2673.6(9)
Z	4
$D_c/g\ cm^{-3}$	1.861
$\mu(\text{Mo-K}\alpha)/\text{mm}^{-1}$	1.765
$F(000)$	1448
Goodness-of-fit on F^2	1.080
$R_1 [I > 2\sigma(I)]/(\text{all})$	0.0616/0.0745
$wR_2 [I > 2\sigma(I)]/(\text{all})$	0.1775/0.1896

3. Results and Discussion

3.1. Synthetic Procedure

The ruthenium(III) precursor $K_2[RuCl_5(H_2O)]$ was made to react with guanine in hydrochloric acid (3.0 M) solutions, thus we prepared a new purine-based ruthenium(III) complex of the formula $[Ru(\mu-Cl)(\mu-gua)_2Cl_4] \cdot 2H_2O$ (**1**) (Figure 1). The synthetic procedure was carried out by means of heating this mixture at 90 °C in a solvothermal reaction and, in order to crystallize, the process continued for a further 12 h cooling step to room temperature. In this way, dark brown crystals of **1** were obtained with a satisfactory yield (53%). It is worth mentioning that compound **1** was also obtained by replacing hydrochloric acid with acetic acid, but the yield was too low (less than 10%). These results support the fact that this is an adequate synthesis to prepare purine-based dinuclear ruthenium(III) complexes.

3.2. Infrared Spectroscopy

The infrared (IR) spectra of **1** and that of the free guanine ligand are given in Figure 2. The IR spectrum of guanine has been previously studied [31,32], so that it has been added in this work only for comparison. In general, the vibrational bands mainly associated with N-H symmetric (ν_s) and asymmetric (ν_{as}) stretching for the free guanine molecule were more intense and complex than those of **1** in the ca. 3800–2000 cm^{-1} region (Figure 2), which would be due to a more ordered hydrogen-bonding network in the crystalline solid for the free nucleobase [31,32]. In the case of the IR spectrum of **1**, the values associated to the vibrational $\nu_{as}(NH_2)$ (3325 cm^{-1}) and $\nu_s(NH_2)$ (3114 and 3062 cm^{-1}) bands were very similar to those obtained for the free guanine [31,32] (Figure 2). In the 1800–500 cm^{-1} region, the most interesting features were the two strong vibrational bands associated to the stretching $\nu(C=N)$ and $\nu(C=C)$ and bending $\delta(NH_2)$, mainly scissoring, which were found at 1695 and 1672 cm^{-1} for the guanine molecule [31,32]. In the IR spectrum of **1**, these two vibrational bands were shifted to 1708 and 1635 cm^{-1} , respectively, with this fact indicating the coordination of the Ru(III) metal ions to guanine molecules in compound **1** (Figure 2).

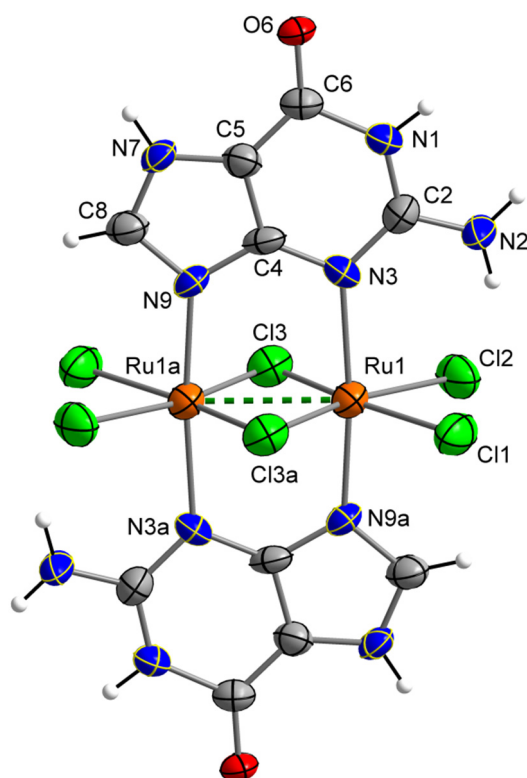


Figure 1. Molecular structure of the neutral $[\text{Ru}(\mu\text{-Cl})(\mu\text{-gua})_2\text{Cl}_4]$ complex in **1** along with the atom labels scheme, the green-dashed line indicating a metal–metal bond. Water molecules have been omitted for clarity.

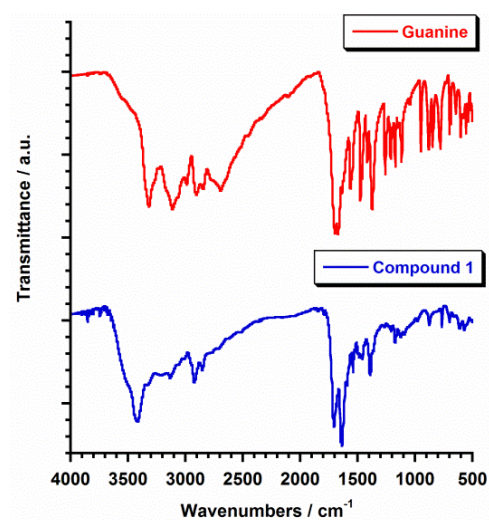


Figure 2. FT-IR spectra for guanine (red) and compound **1** (blue).

3.3. Description of the Crystal Structure

The crystal structure of **1** was obtained by single-crystal X-ray diffraction. A CSD survey revealed that **1** displays the first reported crystal structure based on a dinuclear Ru(III) compound containing guanine. Compound **1** crystallizes in the monoclinic system with space group $C2/c$ (Table 1). The crystal structure of **1** is made up of neutral $[\text{Ru}(\mu\text{-Cl})(\mu\text{-gua})_2\text{Cl}_4]$ units and H_2O molecules. The asymmetric unit of **1** consists of half a $[\text{Ru}(\mu\text{-Cl})(\mu\text{-gua})_2\text{Cl}_4]$ complex and one H_2O molecule (Figure 1).

In this dinuclear complex, each Ru(III) ion is linked to four chloride ions and two nitrogen atoms (these are N3 and N9) from two guanine molecules in an almost regular Oh geometry. The two Ru(III) ions are connected to each other through two guanine molecules and two chloro-bridges (Figure 1). A very short intramolecular Ru···Ru distance [$\text{Ru}(1)\cdots\text{Ru}(1a) = 2.644 \text{ \AA}$, $(a) = -x-1/2, -y+1/2, -z-2$] indicates the formation of a metal–metal bond (dashed line in Figure 1). The average values of the Ru–Cl [$2.318(1) \text{ \AA}$] and Ru–N [$2.103(1) \text{ \AA}$] bond lengths are in agreement with those values published for previously reported Ru(III) systems with a similar metal environment [17,25].

In the crystal of **1**, H-bonding interactions between neighboring guanine molecules [$\text{O}(6)\cdots\text{N}(7b)$ distance of ca. $2.745(1) \text{ \AA}$, $(b) = -x, -y, -z-1$] afford chains of neutral $[\{\text{Ru}(\mu\text{-Cl})(\mu\text{-gua})\}_2\text{Cl}_4]$ units (Figure 3). These chains are linked by additional H-bonds involving Cl^- anions and NH_2 groups of adjacent guanine molecules [$\text{Cl}(3)\cdots\text{N}(2c)$ distance of ca. $3.345(1) \text{ \AA}$, $(c) = -x-1/2, y-1/2, -z-3/2$], which set up a two-dimensional network. The cohesiveness of the structure is further strengthened by the presence of intermolecular $\text{Cl}\cdots\pi$ interactions among $[\{\text{Ru}(\mu\text{-Cl})(\mu\text{-gua})\}_2\text{Cl}_4]$ units [$\text{Cl}\cdots\pi$ interactions ranging with $3.52\text{--}3.81 \text{ \AA}$ values]. The thus packed $[\{\text{Ru}(\mu\text{-Cl})(\mu\text{-gua})\}_2\text{Cl}_4]$ units generate cavities with a diameter of ca. 13 \AA , where most of the water molecules are located in **1** (Figure 4). The supramolecular network is supported by additional H-bonding interactions, which stabilize the crystal structure in compound **1**.

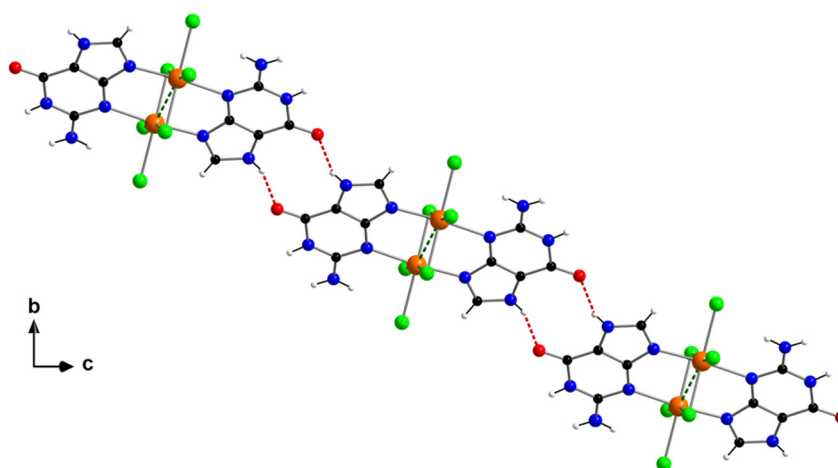


Figure 3. View along the crystallographic a axis of a fragment of the crystal packing of **1**. H-bonding interactions between O atoms and N-H groups of adjacent $[\{\text{Ru}(\mu\text{-Cl})(\mu\text{-gua})\}_2\text{Cl}_4]$ units are shown as red-dashed lines. Water molecules have been omitted for clarity.

3.4. Hirshfeld Surface Analysis

The intermolecular interactions of the neutral $[\{\text{Ru}(\mu\text{-Cl})(\mu\text{-gua})\}_2\text{Cl}_4]$ complex were further studied through the CrystalExplorer program [33,34]. This program calculated the surfaces which allowed us the qualitative and quantitative investigation as well as the visualization of the main intermolecular contacts in **1** by mapping the distances from the surface to the nearest atom outside (d_e) and inside (d_i) this surface. Besides, a normalized contact distance called d_{norm} was also taken into account to overcome some limitations generated by the atom size [33,34]. The Hirshfeld surfaces for complex **1** are given in Figure 5, the shorter contacts being shown with red color [34]. The intermolecular $\text{H}\cdots\text{O}$ contacts generated among the N-H and carbonyl groups of adjacent guanine molecules are approximately 16% of the complete fingerprint plot (Figure 5). The $\text{Cl}\cdots\text{H}$ contacts involving Cl^- anions and N-H groups of neighboring dinuclear $[\{\text{Ru}(\mu\text{-Cl})(\mu\text{-gua})\}_2\text{Cl}_4]$ units are the main interactions observed on the Hirshfeld surface, which covers ca. 24% (Figure 5). Finally, further $\text{O}\cdots\text{H}$ contacts involving solvent water molecules and N-H groups of the guanine molecules are close to the 6% of the fingerprint plot (Figure 5).

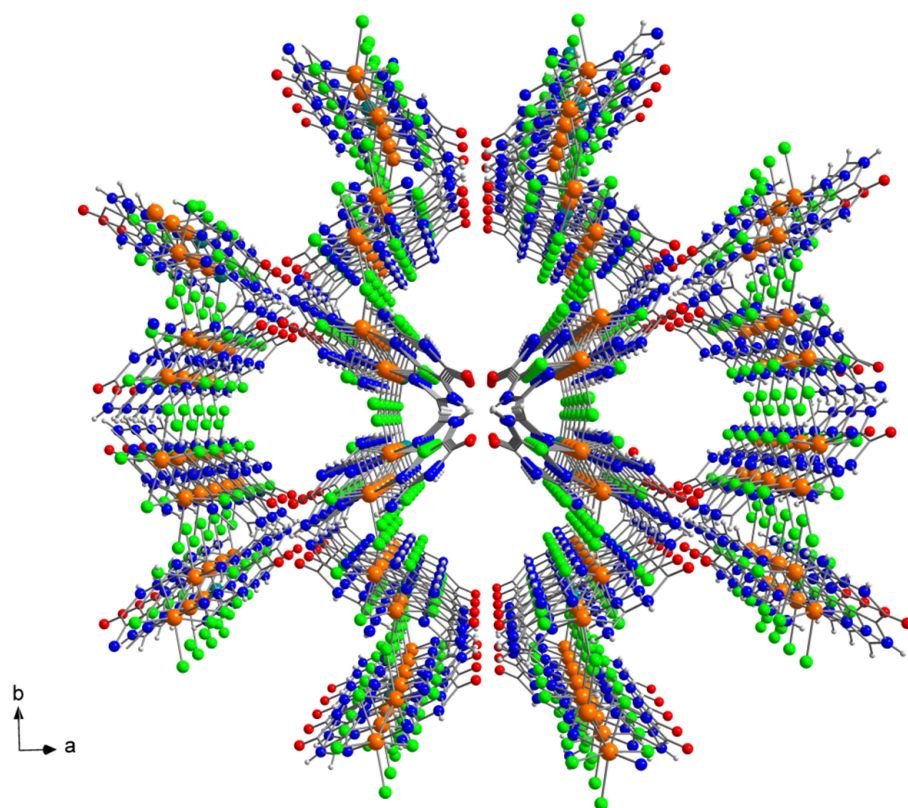


Figure 4. View along the crystallographic c axis of a fragment of the crystal packing of **1**. Water molecules have been omitted for clarity.

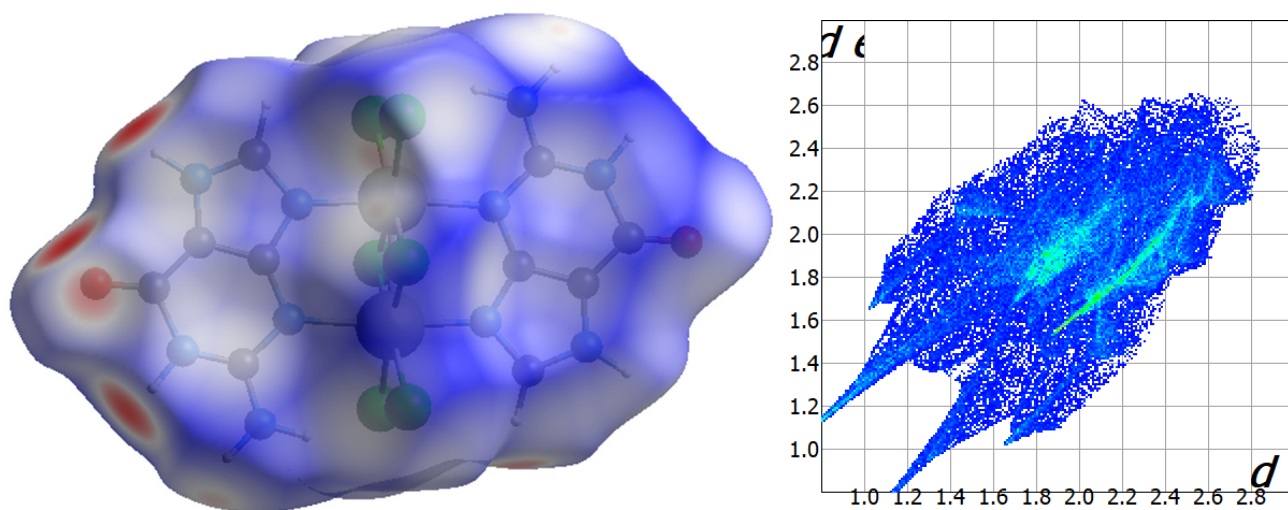
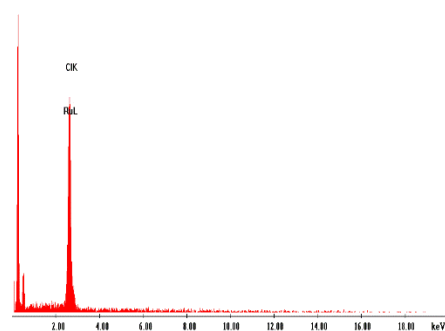


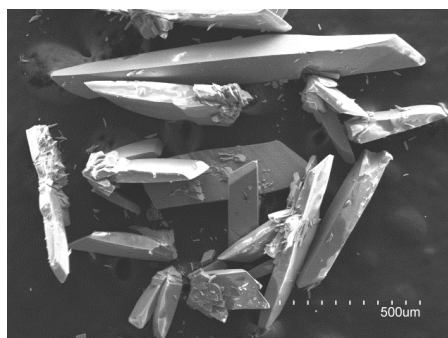
Figure 5. Hirshfeld surface mapped with d_{norm} function for **1** (left); Full fingerprint plot for the dinuclear Ru(III) complex of **1** (right).

3.5. Scanning Electron Microscopy–Energy Dispersive X-ray Analysis

Compound **1** was studied by means of scanning electron microscopy and energy dispersive X-ray analysis (SEM-EDX), these analyses being carried out as previously performed for other ruthenium systems [35,36]. The results of the microanalysis gave a Ru/Cl molar ratio of 1:3 for **1**. A recorded image of **1** is given in Figure 6. Crystals of **1** are shown as crystallized parallelepipeds in Figure 6.



(a)



(b)

Figure 6. Energy dispersive X-ray analysis (EDX) spectrum for **1** (a); scanning electron microscopy (SEM) image of crystals of **1** (b).

3.6. Cyclic Voltammetry (CV)

The study of the electrochemical properties of compound **1** was performed employing cyclic voltammetry (CV) in *N,N'*-dimethylformamide (DMF), containing 0.1 M $[\text{NBu}_4][\text{PF}_6]$, in the range of potential values of +1.5 and -1.5 V and at 20 °C. The CV curve for **1** is shown in Figure 7.

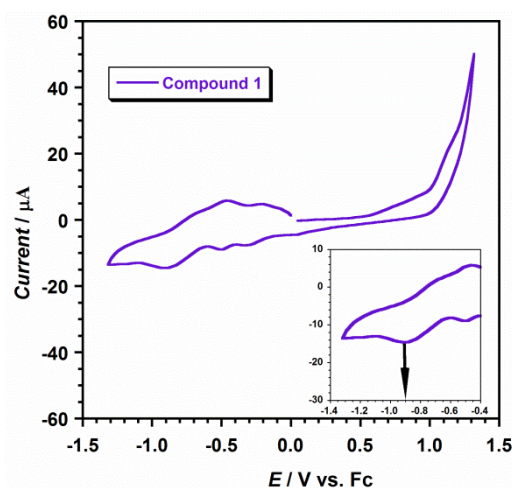


Figure 7. Cyclic voltammogram of **1** in a dry DMF 10^{-3} M solution (with 0.1 M $[\text{NBu}_4][\text{PF}_6]$) at 20 °C and scan rate 200 mV/s. The area of the working electrode is 0.32 cm^2 .

Dinuclear ruthenium compounds containing metal–metal bonds have been studied for many years [37]. They show redox properties that are strongly dependent upon the solvent and the supporting electrolyte and are generally well known [38–40]. So, this type of Ru–Ru compound could be an acceptable reference in electrochemical studies [38–40].

In the CV curve of **1**, three reduction processes can be observed (Figure 7). The first two reduction peaks were found between 0.0 V and -0.50 V, which would be associated with the formation of the mixed-valent Ru(II)-Ru(III) species (at -0.30 V) and also to that of the Ru(II)-Ru(II) system (at -0.50 V). These reduction potential values are close to those published for other dinuclear ruthenium complexes [38–40]. Nevertheless, much more interesting would be the third detected reduction peak at -0.89 V, which would be generated by the influence of the guanine molecule, see inset in Figure 7. It is worth mentioning that this value assigned to guanine is in agreement with those previously reported for this purine nucleobase in electrochemistry research works performed through modified electrodes based on polyaniline-MnO₂ [41] and graphite-WS₂ [42], which have shown high accuracy and promising redox activity toward purine nucleobases [41,42]. In order to analyze the repeatability of the CV curve, it was measured five times. Indeed, a relative standard deviation value of ca. 1.2% for the current response was obtained for **1**. In any case, these results could establish a first step to develop new sensor devices suitable for the detection of purine nucleobases as guanine [25]. Nevertheless, this is an early stage of the research and, therefore, this type of diruthenium(III) systems must be further investigated. The comparison with other methods together with the study of the nature of the samples to be measured will be addressed subsequently in future works [25].

4. Conclusions

An unusual guanine-based dinuclear ruthenium(III) complex, of the formula $[\{\text{Ru}(\mu\text{-Cl})(\mu\text{-gua})\}_2\text{Cl}_4]\cdot 2\text{H}_2\text{O}$ (**1**) (gua = guanine), was prepared and characterized. Compound **1** is the first dinuclear ruthenium(III) compound based on guanine reported so far. Compound **1** was characterized by FT-IR, SEM-EDX, single-crystal X-ray diffraction (XRD), Hirshfeld surface analysis and cyclic voltammetry (CV). The study of its electrochemical properties revealed well-resolved, potentially useful, current peaks, which allowed us to investigate the guanine when linked to the ruthenium ion in **1**.

Supplementary Materials: The following supporting information can be downloaded at: <https://www.mdpi.com/article/10.3390/cryst12040448/s1>, X-ray crystallographic data in CIF format for compound **1**.

Author Contributions: Conceptualization, I.C. and J.M.-L.; funding acquisition, I.C. and J.M.-L.; methodology, M.O.-A., A.S.-L., I.C. and J.M.-L.; investigation, M.O.-A., A.S.-L., I.C. and J.M.-L.; formal analysis, M.O.-A., A.S.-L., I.C. and J.M.-L.; writing—original draft preparation, J.M.-L.; writing—review and editing, J.M.-L. All authors have read and agreed to the published version of the manuscript.

Funding: This research was funded by Spanish Ministry of Science and Innovation (Grant number PID2019-109735GB-I00) and also by VLC-BIOCLINIC Program of the University of Valencia (Grant number PI-2021-007-DIRUGEN).

Institutional Review Board Statement: Not applicable.

Informed Consent Statement: Not applicable.

Data Availability Statement: The raw data that support the findings of this study are available from the corresponding author upon reasonable request.

Acknowledgments: M.O.-A. thanks the Spanish “FPI” PhD funding action plan.

Conflicts of Interest: The authors declare no conflict of interest.

References

1. An, S.; Kumar, R.; Sheets, E.D.; Benkovic, S.J. Reversible Compartmentalization of de Novo Purine Biosynthetic Complexes in Living Cells. *Science* **2008**, *320*, 103–106. [[CrossRef](#)] [[PubMed](#)]
2. Pedley, A.M.; Benkovic, S.J. A New View into the Regulation of Purine Metabolism—The Purinosome. *Trends Biochem. Sci.* **2017**, *42*, 141–154. [[CrossRef](#)] [[PubMed](#)]
3. Rhodes, D.; Lipps, H.J. G-quadruplexes and their regulatory roles in biology. *Nucleic Acids Res.* **2015**, *43*, 8627–8637. [[CrossRef](#)]

4. Huynh, R.A.; Mohan, C. Alzheimer's Disease: Biomarkers in the Genome, Blood, and Cerebrospinal Fluid. *Front. Neurol.* **2017**, *8*, 102. [[CrossRef](#)] [[PubMed](#)]
5. Beamer, E.; Lacey, A.; Alves, M.; Conte, G.; Tian, F.; de Diego-García, L.; Khalil, M.; Rosenow, F.; Delanty, N.; Dale, N.; et al. Elevated blood purine levels as a biomarker of seizures and epilepsy. *Epilepsia* **2021**, *62*, 817–828. [[CrossRef](#)]
6. Kolgiri, V.; Patil, V.W. Protein carbonyl content: A novel biomarker for aging in HIV/AIDS patients. *Braz. J. Infect. Dis.* **2017**, *21*, 35–41. [[CrossRef](#)]
7. Ellis, R.J.; Moore, D.J.; Sundermann, E.E.; Heaton, R.K.; Mehta, S.; Hulgán, T.; Samuels, D.; Fields, J.A.; Letendre, S.L. Nucleic acid oxidation is associated with biomarkers of neurodegeneration in CSF in people with HIV. *Neurol. Neuroimmunol. Neuroinflamm.* **2020**, *7*, e902. [[CrossRef](#)]
8. Klampfl, C.W.; Himmelsbach, M.; Buchberger, W.; Klein, H. Determination of purines and pyrimidines in beer samples by capillary zone electrophoresis. *Anal. Chim. Acta* **2002**, *454*, 185–191. [[CrossRef](#)]
9. Inazawa, K.; Sato, A.; Kato, Y.; Yamaoka, N.; Fukuuchi, T.; Yasuda, M.; Mawatari, K.; Nakagomi, K.; Kaneko, K. Determination and profiling of purines in foods by using HPLC and LC-MS. *Nucleosides Nucleotides Nucleic Acids* **2014**, *33*, 439–444. [[CrossRef](#)]
10. Higgins, S. Regarding ruthenium. *Nat. Chem.* **2010**, *2*, 1100. [[CrossRef](#)]
11. Bruneau, C.; Achard, M. Allylic ruthenium(IV) complexes in catalysis. *Coord. Chem. Rev.* **2012**, *256*, 525–536. [[CrossRef](#)]
12. Furrer, J.; Süß-Fink, G. Thiolato-bridged dinuclear arene ruthenium complexes and their potential as anticancer drugs. *Coord. Chem. Rev.* **2016**, *309*, 36–50. [[CrossRef](#)]
13. Zeng, L.; Gupta, P.; Chen, Y.; Wang, E.; Ji, L.; Chao, H.; Chen, Z.-S. The development of anticancer ruthenium(II) complexes: From single molecule compounds to nanomaterials. *Chem. Soc. Rev.* **2017**, *46*, 5771–5804. [[CrossRef](#)]
14. Alessio, E. Thirty Years of the Drug Candidate NAMI-A and the Myths in the Field of Ruthenium Anticancer Compounds: A Personal Perspective. *Eur. J. Inorg. Chem.* **2017**, 1549–1560. [[CrossRef](#)]
15. Alessio, E.; Messori, L. NAMI-A and KP1019/1339, Two Iconic Ruthenium Anticancer Drug Candidates Face-to-Face: A Case Story in Medicinal Inorganic Chemistry. *Molecules* **2019**, *24*, 1995. [[CrossRef](#)]
16. Chen, H.; Parkinson, J.A.; Parsons, S.; Coxall, R.A.; Gould, R.O.; Sadler, P.J. Organometallic Ruthenium(II) Diamine Anticancer Complexes: Arene-Nucleobase Stacking and Stereospecific Hydrogen-Bonding in Guanine Adducts. *J. Am. Chem. Soc.* **2002**, *124*, 3064–3082. [[CrossRef](#)]
17. Armentano, D.; Martínez-Lillo, J. Hexachlororhenate(IV) salts of ruthenium(III) cations: X-ray structure and magnetic properties. *Inorg. Chim. Acta* **2012**, *380*, 118–124. [[CrossRef](#)]
18. Orts-Arroyo, M.; Castro, I.; Lloret, F.; Martínez-Lillo, J. Molecular Self-Assembly in a Family of Oxo-Bridged Dinuclear Ruthenium(IV) Systems. *Cryst. Growth Des.* **2020**, *20*, 2044–2056. [[CrossRef](#)]
19. Escrivà, E.; García-Lozano, J.; Martínez-Lillo, J.; Nuñez, H.; Server-Carrió, J.; Soto, L.; Carrasco, R.; Cano, J. Synthesis, Crystal Structure, Magnetic Properties, and Theoretical Studies of $[\{\text{Cu}(\text{mepirizole})\text{Br}\}_2(\mu\text{-OH})(\mu\text{-pz})]$ (Mepirizole = 4-Methoxy-2-(5-methoxy-3-methyl-1H-pyrazol-1-yl)-6-methylpyrimidine; pz = Pyrazolate), a Novel μ -Pyrazolato- μ -Hydroxo-Dibridged Copper(II) Complex. *Inorg. Chem.* **2003**, *42*, 8328–8336.
20. Armentano, D.; Marino, N.; Mastropietro, T.F.; Martínez-Lillo, J.; Cano, J.; Julve, M.; Lloret, F.; De Munno, G. Self-Assembly of a Chiral Carbonate- and Cytidine-Containing Dodecanuclear Copper(II) Complex: A Multiarm-Supplied Globular Capsule. *Inorg. Chem.* **2008**, *47*, 10229–10231. [[CrossRef](#)]
21. Marino, N.; Armentano, D.; Mastropietro, T.F.; Julve, M.; De Munno, G.; Martínez-Lillo, J. Cubane-Type Cu^{II}_4 and $\text{Mn}^{\text{II}}_2\text{Mn}^{\text{III}}_2$ Complexes Based on Pyridoxine: A Versatile Ligand for Metal Assembling. *Inorg. Chem.* **2013**, *52*, 11934–11943. [[CrossRef](#)] [[PubMed](#)]
22. Armentano, D.; Barquero, M.A.; Rojas-Dotti, C.; Moliner, N.; De Munno, G.; Brechin, E.K.; Martínez-Lillo, J. Enhancement of Intermolecular Magnetic Exchange through Halogen...Halogen Interactions in Bisadeninium Rhenium(IV) Salts. *Cryst. Growth Des.* **2017**, *17*, 5342–5348. [[CrossRef](#)]
23. Orts-Arroyo, M.; Castro, I.; Lloret, F.; Martínez-Lillo, J. Field-induced slow relaxation of magnetisation in two one-dimensional homometallic dysprosium(III) complexes based on alpha- and beta-amino acids. *Dalton Trans.* **2020**, 49, 9155–9163. [[CrossRef](#)] [[PubMed](#)]
24. Orts-Arroyo, M.; Ten-Esteve, A.; Ginés-Cárdenas, S.; Castro, I.; Martí-Bonmatí, L.; Martínez-Lillo, J. A gadolinium(III) complex based on the thymine nucleobase with properties suitable for magnetic resonance imaging. *Int. J. Mol. Sci.* **2021**, *22*, 4586. [[CrossRef](#)] [[PubMed](#)]
25. Orts-Arroyo, M.; Castro, I.; Martínez-Lillo, J. Detection of Hypoxanthine from Inosine and Unusual Hydrolysis of Immunosuppressive Drug Azathioprine through the Formation of a Diruthenium(III) System. *Biosensors* **2021**, *11*, 19. [[CrossRef](#)] [[PubMed](#)]
26. Sanchis-Perucho, A.; Orts-Arroyo, M.; Camús-Hernández, J.; Rojas-Dotti, C.; Escrivà, E.; Lloret, F.; Martínez-Lillo, J. Hexachlororhenate(IV) salts of protonated ciprofloxacin: Antibiotic-based single-ion magnets. *CrystEngComm* **2021**, *23*, 8579–8587. [[CrossRef](#)]
27. Orts-Arroyo, M.; Sanchis-Perucho, A.; Moliner, N.; Castro, I.; Lloret, F.; Martínez-Lillo, J. One-Dimensional Gadolinium (III) Complexes Based on Alpha- and Beta-Amino Acids Exhibiting Field-Induced Slow Relaxation of Magnetization. *Inorganics* **2022**, *10*, 32. [[CrossRef](#)]
28. Turel, I.; Pecanac, M.; Golobic, A.; Alessio, E.; Serli, B.; Bergamo, A.; Sava, G. Solution, solid state and biological characterization of ruthenium(III)-DMSO complexes with purine base derivatives. *J. Inorg. Biochem.* **2004**, *98*, 393–401. [[CrossRef](#)]
29. SHELXTL-2017/1, Bruker Analytical X-ray Instruments; Bruker: Madison, WI, USA, 2017.

30. DIAMOND 4.5.0, *Crystal Impact GbR.*; Crystal Impact: Bonn, Germany, 2018.
31. Sheina, G.G.; Stepanian, S.G.; Radchenko, E.D.; Blagoi, Y.P. IR spectra of guanine and hypoxanthine isolated molecules. *J. Mol. Struct.* **1987**, *158*, 275–292. [[CrossRef](#)]
32. Beć, K.B.; Grabska, J.; Czarnecki, M.A.; Huck, C.W.; Wójcik, M.J.; Nakajima, T.; Ozaki, Y. IR Spectra of Crystalline Nucleobases: Combination of Periodic Harmonic Calculations with Anharmonic Corrections Based on Finite Models. *J. Phys. Chem. B* **2019**, *123*, 10001–10013. [[CrossRef](#)]
33. Spackman, M.A.; Jayatilaka, D. Hirshfeld surface analysis. *CrystEngComm* **2009**, *11*, 19–32. [[CrossRef](#)]
34. Turner, M.J.; McKinnon, J.J.; Wolff, S.K.; Grimwood, D.J.; Spackman, P.R.; Jayatilaka, D.; Spackman, M.A. *Crystal Explorer 17*; University of Western Australia: Perth, Australia, 2017.
35. Mohite, S.S.; Patil-Deshmukh, A.B.; Chavan, S.S. Synthesis and characterization of Ru(III) complexes with 2-((E)-((4-(4-bromophenyl)ethynyl)phenyl)imino)methyl-4-((E)-phenyldiazenyl)phenol and their use as a precursor for RuO₂ nanoparticles. *J. Mol. Struct.* **2019**, *1176*, 386–393. [[CrossRef](#)]
36. Sur, V.P.; Mazumdar, A.; Kopel, P.; Mukherjee, S.; Vitek, P.; Michalkova, H.; Vaculovičová, M.; Moulick, A. A Novel Ruthenium Based Coordination Compound Against Pathogenic Bacteria. *Int. J. Mol. Sci.* **2020**, *21*, 2656. [[CrossRef](#)] [[PubMed](#)]
37. Cotton, F.A.; Pedersen, E. Magnetic and electrochemical properties of transition metal complexes with multiple metal-to-metal bonds. II. Tetrabutyratodiruthenium(n+) with n = 0 and 1. *Inorg. Chem.* **1975**, *14*, 388–391. [[CrossRef](#)]
38. Malinski, T.; Chang, D.; Feldmann, F.N.; Bear, J.L.; Kadish, K.M. Electrochemical studies of a novel ruthenium(II,III) dimer, trifluoroacetamidatoruthenium chloride (Ru₂(HNOCCF₃)₄Cl). *Inorg. Chem.* **1983**, *22*, 3225–3233. [[CrossRef](#)]
39. Hiraoka, Y.; Ikeue, T.; Sakiyama, H.; Guégan, F.; Luneau, D.; Gillon, B.; Hiromitsu, I.; Yoshioka, D.; Mikuriya, M.; Kataoka, Y.; et al. An unprecedented up-field shift in the ¹³C NMR spectrum of the carboxyl carbons of the lantern-type dinuclear complex TBA[Ru₂(O₂CCH₃)₄Cl₂] (TBA⁺ = tetra(n-butyl)ammonium cation). *Dalton Trans.* **2015**, *44*, 13439–13443. [[CrossRef](#)]
40. Kataoka, Y.; Mikami, S.; Sakiyama, H.; Mitsumi, M.; Kawamoto, T.; Handa, M. A neutral paddlewheel-type diruthenium(III) complex with benzamidinato ligands: Synthesis, crystal structure, magnetism, and electrochemical and absorption properties. *Polyhedron* **2017**, *136*, 87–92. [[CrossRef](#)]
41. Prathap, M.U.A.; Srivastava, R.; Satpati, B. Simultaneous detection of guanine, adenine, thymine, and cytosine at polyaniline/MnO₂ modified electrode. *Electrochim. Acta* **2013**, *114*, 285–295. [[CrossRef](#)]
42. Zhang, J.; Han, D.; Wang, S.; Zhang, X.; Yang, R.; Ji, Y.; Yu, X. Electrochemical detection of adenine and guanine using a three-dimensional WS₂ nanosheet/graphite microfiber hybrid electrode. *Electrochem. Commun.* **2019**, *99*, 75–80. [[CrossRef](#)]